International Journal of Biological Macromolecules 141 (2019) 504–510

Contents lists available at ScienceDirect

International Journal of Biological Macromolecules

journal homepage: http://www.elsevier.com/locate/ijbiomac

Alginate films functionalized with silver sulfadiazine-loaded [Mg-Al] layered double hydroxide as antimicrobial wound dressing

Davi R. Munhoz [a], Marcela P. Bernardo [a,*], João O.D. Malafatti [a,b], Francys K.V. Moreira [c], Luiz H.C. Mattoso [a]

[a] National Nanotechnology Laboratory for Agriculture (LNNA), Embrapa Instrumentation, 1452 XV de Novembro St., 13560-970 São Carlos, SP, Brazil
[b] Department of Chemistry, Federal University of São Carlos, Rod. Washington Luís, Km 235, 13565-905 São Carlos, SP, Brazil
[c] Department of Materials Engineering, Federal University of São Carlos, Rod. Washington Luís, Km 235, 13565-905 São Carlos, SP, Brazil

ARTICLE INFO

Article history:
Received 27 May 2019
Received in revised form 29 August 2019
Accepted 4 September 2019
Available online 04 September 2019

Keywords:
Continuous casting
Bionanocomposites
Burn wounds

ABSTRACT

Alginate (ALG) is an abundant, biocompatible, regenerative, and nontoxic polysaccharide that has potential applications in tissue engineering. Silver sulfadiazine (SDZ) is a topical antibiotic used to control bacterial infection in burns. Aiming to combine the intrinsic alginate characteristics and silver sulfadiazine antimicrobial properties, hydrotalcite ([Mg-Al]-LDH) was used as a host matrix to obtain a system efficient in delivering SDZ from alginate films. SDZ was successfully intercalated in [Mg-Al]-LDH through structural reconstruction. Different solutions were prepared using sodium alginate at 10 wt%, glycerol at 10 wt% as a plasticizer and [Mg-Al]-LDH and [Mg-Al]-LDH/SDZ as fillers at 1 wt% and 5 wt%. Films were obtained by continuous casting and further characterized for their microstructural, mechanical, water barrier and antimicrobial properties. Cytotoxicity tests were also performed on fibroblasts cells. The incorporation of [Mg-Al]-LDH and [Mg-Al]-LDH/SDZ presented neither negative nor positive effects on the mechanical properties and morphology of the alginate films. Moreover, samples containing SDZ exhibited inhibitory activity against *S. aureus*, *E. coli*, and *S. enterica*. The addition of [Mg-Al]-LDH/SDZ even at the highest concentration did not afford a very significant cytotoxicity to the alginate-[Mg-Al]-LDH/SDZ films. These results describe a suitable approach for preparing innovative active wound dressings integrated to efficient drug delivery.

1. Introduction

Human skin, the largest organ of the body, is essential for physical protection, sensory touch, thermoregulation, fluid homeostasis and immune surveillance [1,2]. Different injuries may occur on Human skin and can be classified based on their damaging potential either as acute or chronic. Injuries caused by external factors, such as abrasion, tears and mechanical injuries are classified as acute wounds, which usually heal completely with minimal scarring within an expected period of about 8–12 weeks [3,4]. On the other hand, repeated tissue injuries or diseases (e.g. diabetes) lead to chronic wounds, which heal slowly (longer than 12 weeks) and often reoccur [5].

Burn is an injury classified as an acute wound as a result of exposure to heat or radiation, radioactivity, electricity, friction or contact with chemicals. According to the World Health Organization, the US costs for children care with burn injuries exceeded US$ 211 million in 2000. In Norway, the management costs of burn hospitals exceeded €10.5 million in 2007, and in South Africa, around US$ 26 million is spent annually for care of burn injuries [6].

Interactive wound dressing acts on the healing process due to the presence of bioactive agents that influence on physiological processes and foment the healing cascade [7]. In addition, wound dressing prevents loss of body fluid, protecting the wounds from external contamination, mainly caused by microorganisms [8]. Different biopolymers, such as chitosan, alginate and fucoidan, may be used to obtain wound dressings. Alginate is a naturally occurring, anionic polysaccharide that is extracted from brown sea algae and contains two uronic acids, namely, (β 1,4)-linked d-mannuronic acid (M) and α-(1-4) linked l-guluronic acid (G), being composed of homopolymer chains M–M or G–G and chain segments with an alternating sequence of M–G blocks [9]. Alginate has singular characteristics that make it a potential and important biopolymer for wound healing applications, including non-toxicity, biodegradability, biocompatibility and non-immunogenicity [10]. Moreover, alginate can absorb wound fluid, promoting a dry wound with a physiologically stable environment that stimulates tissue healing [11].

Burn injuries destroy the skin barrier that prevents microorganism growth [12]. One of the main strategies against bacterial infection in wounds is the use of antimicrobial noble metals. Ionic silver (Ag^+) has a broad-spectrum biocidal activity due to its capability of binding electrostatically to structural N- and S-groups of proteins and other biomolecules present in the bacteria cell membrane, which leads to its lysis.

* Corresponding author.
E-mail address: marcelapiassib@gmail.com (M.P. Bernardo).

https://doi.org/10.1016/j.ijbiomac.2019.09.019
0141-8130/

Ag^+ ions can also penetrate microbial cells through several pathways and interfere on both ribosomes and DNA dynamics by reactive oxygen species (ROS), also resulting in bacteria cell death [13,14].

Local delivery of antimicrobial agents, e.g. silver, is less invasive than a systemic administration. In fact, combining wound dressing to gradual delivery of antimicrobial agents provides tissue compatibility, minimizing the occurrence of bacterial resistance and interference on wound healing [4]. However, the direct application of silver in the wound may be toxic for epithelial cells. In this sense, layered double hydroxides are excellent candidates to delivery Ag^+ ions at an adequate and gradual rate to the wound.

Layered double hydroxides (LDH) are a class of inorganic materials of general formulae $[M^{2+}_{1-x}\, M^{3+}_{x}\, (OH)_2]^{x+}[A^{n-}]_{x/n}\, yH_2O$, whose crystalline structure is based on the brucite-like sheets, where the bivalent cations (M^{2+}) are isomorphic replaced with trivalent cations (M^{3+}). The positive charge excess in the LDH structure is counter-balanced by the intercalation of anionic species (A^{n-}) in the hydrated interlayer regions, and x is the molar ratio $M^{3+}/(M^{3+} + M^{2+})$, ranging from 0.1 to 0.5 [15,16]. The nature of the interlayer A^{n-} species varies between anions, inorganic molecules and organic molecules, including oligonucleotides and genetic materials, such as DNA and RNA [17–20]. LDH also present excellent ion exchange properties, enabling them to be used as a matrix for gradual or controlled release of anionic substances.

Although antimicrobial drug-loaded LDH have been extensively disclosed in the literature, there are no reports on the combination of silver sulfadiazine (SDZ), a topical antibiotic used in patients with burn to prevent infections, with LDH in alginate films aiming at antimicrobial wound dressing applications. Herein, this study describes a suitable approach for the preparation of an innovative active wound dressing based on alginate films loaded with SDZ-intercalated [Mg-Al]-LDH to act as an efficient and biocompatible system to delivery an antimicrobial agent on burn wounds.

2. Materials and methods

2.1. Materials

Sodium alginate extracted from brown algae (η = 5.0–40.0 cps, c_{water} = 1%, at 25 °C) and silver (I) sulfadiazine ($C_{10}H_9AgN_4O_2S$, 98%) were purchased from Sigma-Aldrich (St. Louis, MO, USA). Hydrotalcite (PURAL® MG 61 HT) was kindly donated by Sasol – Germany GmbH. All reagents were used as received. Decarbonated ultra-pure H_2O (ρ = 18.2 MΩ cm) obtained by a Milli-Q system (Barnstead Nanopure Diamond, Thermo Fisher Scientific Inc., Dubuque, IA, USA) was used exclusively in all experimental procedures.

2.2. Methods

2.2.1. Intercalation of silver sulfadiazine in hydrotalcite

The SDZ-intercalated [Mg-Al]-LDH samples were prepared using the structural reconstruction method [21]. Briefly, the [Mg-Al]-LDH was thermally treated at 600 °C for 4 h. Subsequently, 500 mg of the calcined product were added to 250 mL of six different aqueous SDZ solutions (0.008 g L^{-1}; 0.1 g L^{-1} and 0.25 g L^{-1}) at 25 °C under continuous agitation to reconstruct the LDH. After 24 h, the samples were centrifuged at 11.200 *g* for 10 min and washed with methanol to remove the SDZ excess and finally dried overnight at 45 °C. Samples were labelled as [Mg-Al]-LDH/SDZ when reconstructed in SDZ solution. [Mg-Al]-LDH was also reconstructed in ultrapure water and used as a control.

2.2.2. Preparation of alginate-[Mg-Al]-LDH/SDZ films by continuous casting

Five different alginate-based films were prepared in this study, as shown in Table 1. First, the LDH sample (either [Mg-Al]-LDH or [Mg-Al]-LDH/SDZ) was added to ultrapure water and sonicated at amplitude of 50% (450 Branson sonifier, tapped step horn 1/2″ tip diameter) for 10 min to form a filler dispersion. Then, sodium alginate (10 wt%) and glycerol (10 wt%) were added to the dispersion, which was further homogenized in a vacuum mixer running at 2000 rpm and −300 mmHg [22]. A pure solution (ALG-G) was also prepared by directly solubilizing alginate and glycerol in ultrapure water using the vacuum mixer.

Table 1
Compositions of alginate-based film samples prepared in this study.

Samples[a]	Alginate (wt%)	Mg-Al-LDH (wt%)[b]	Mg-Al-LDH/SDZ (wt%)[b]
ALG-G (control)	10%	–	–
ALG-G-[Mg-Al]-LDH-1%	10%	1%	–
ALG-G-[Mg-Al]-LDH-5%	10%	5%	–
ALG-G-[Mg-Al]-LDH/SDZ-1%	10%	–	1%
ALG-G-[Mg-Al]-LDH/SDZ-5%	10%	–	5%

[a] All samples were prepared using glycerol as a plasticizer at 10 wt%.
[b] Dried alginate mass basis.

The film samples were prepared by continuous casting (CC) in a KTF-B labcoater machine (Werner Mathis AG, Switzerland), as reported elsewhere [22]. In brief, the formulations were poured onto the moving substrate in the coating device, where a wet layer with thickness of 1.5 mm was formed using a B-type doctor blade and a pair of comparative clocks (±0.001 mm). The wet layer was dried through conveyance at speed of 15 cm min^{-1} by an IR pre-dryer with 42% emission potency and consecutive through one air circulating oven equilibrated at 120 °C. Dried films were then collected at the oven outlet and kept at room temperature for further characterizations.

2.3. Characterizations

Powder X-ray diffraction (PXRD) measurements were conducted on a Shimadzu XRD 6000 diffractometer using Ni-filtered Cu K_α radiation (λ = 1.5405 Å). PXRD patterns were taken over the 2θ range of 3–80° with a scan speed of 1° min^{-1}. Basal spacing (d_{001}) was calculated using the classical Bragg's equation ($n\lambda = 2d\text{sen}\theta$) [21].

Fourier Transform Infrared (FT-IR) analyses were performed using the attenuated total reflectance (ATR) mode on a Bucker spectrometer using spectral resolution of 2 cm^{-1}. Field emission gun scanning electron microscopy (FEG-SEM) was conducted on a JEOL microscope running at 15 kV. Cross-sectional surface of films was prepared by freeze-fracturing in liquid N_2. Powder samples were prepared by deposition of powders on conductive Si wafers. All images were recorded using the secondary electron mode after sample coating with gold (~5 nm) in argon atmosphere. Particle size values were obtained with the Image-J software over 100 single particle measurements.

Tensile tests were carried out following the ASTM D882-09 standard in a universal testing machine EMIC DL3000 (EMIC Equipamento & Ensaio Ltda, PR, Brazil) equipped with a 10 kgf (98 N) load cell. True tensile strength (σ_T), true elongation break (ε_B) and Young's modulus (E) of film samples were determined from stress (σ) – strain (ε) curves. σ_T was calculated as $\sigma_T = \sigma\lambda$, where σ stands for the engineering tensile strength and λ denotes the extensional ratio defined as $\lambda = L/L_0$, where L and L_0 represents the final and initial specimen lengths, respectively. εB was obtained as $\varepsilon_B = \ln\lambda$, while the Young's modulus (E) was determined through linear regression of $\sigma - \varepsilon$ curves in the limit $\sigma = \varepsilon = 0$ ($[d\sigma/d\varepsilon]\varepsilon = 0$). Average film thickness was determined from five random positions in each film using a digital micrometer (Mitutoyo Manufacturing, Japan).

Water vapor permeability (WVP) of films was determined as per ASTM E96 with modifications. Metallic cups were filled with 6 mL of distilled water and further sealed with sample film discs (3 cm in diameter). Average film thickness was also determined from three random positions in each disc using a digital micrometer (Mitutoyo Manufacturing, Japan). The metallic cups were then placed into an air circulation oven at 40 °C containing activated silica gel (RH = 0%) and their mass was periodically registered up to 2 days. WVP was calculated as WVP

= WVT·(ε/ΔP·S), where WVT (g/h) is the water vapor transmission rate calculated by linear regression of the cup mass vs. time curve, ε (m) is the film thickness, S (m^2) is the exposed film area, and ΔP (kPa) is the partial pressure gradient through the film. WVP determinations were performed in triplicate.

2.4. In vitro antimicrobial tests

Antimicrobial activity of pure SDZ, Mg-Al-LDH/SDZ powder, and alginate-based films was tested against *Escherichia coli* (ATCC 11229), *Staphylococcus aureus* (ATCC 6538) and *Salmonella enterica* (NCTC 6017) as per the disc diffusion test methodology [23]. Stock cultures of these microorganisms were kept in falcon tubes at 36 °C during 24 h for cellular growth. The resulting inoculum suspensions were diluted in 0.9% (w/v) NaCl solution, until 0.5 McFarland standard turbidity was matched (108 CFU mL^{-1}). The bacteria were plated with Drigalski spatula onto the solidified Mueller Hinton agar (Becton, Dickinson and Co., Sparks, MD) contained in petri dishes. SDZ and Mg-Al-LDH/SDZ powders (10 mg each) were placed at the center of inoculated Petri dishes, which were incubated for 24 h. Similarly, film disks (D = 2 cm) were exposed to UV light (110 V and 254 nm) for 10 min on each side before being positioned at the midpoint of the inoculated Petri dishes. After 48 h, the Petri dishes were evaluated by observation of inhibitory zones (colony-free areas) and bacterial growth. All tests were done in duplicate.

2.5. Cell culture and toxicity assay by MTT

Human dermal fibroblasts cells (HDFn) were cultivated at 37 °C in humidified 5% CO_2 atmosphere in Dulbecco's modified Eagle medium (DMEM) supplemented with 10% fetal bovine serum (FBS) (v/v). The toxicity assay was conducted according to the ISO 0993-5:2009 standard. For the cytotoxicity assay, cells were seeded at a density of 2 × 10^4 cells per well and stored in a heated chamber overnight before incubation with the sample extract. For the extract, samples were sterilized with UVC (λ = 254 nm) for 15 min each side followed by 24 h incubation in the cell culture medium DMEM red phenol-free supplemented with 5% FBS. The cell medium was replaced with the 24 h-sample-extract and the cells were let in the heated chamber for at least 24 h before the MTT assay. For the MTT assay, the sample-extract medium was replaced by DMEM red phenol-free containing MTT (5 μg/ml) and incubated for 4 h and replaced by 100 μL of DMSO before reading absorbance at 570 nm in a microplate reader (Multiskan™ FC Microplate Photometer – ThermoFisher Scientific). Cells passages were between 4 and 8. All experiments were repeated three times using four well replicates for each time.

2.6. Statistical analysis

Data were subjected to analysis of variance and multiple Duncan or Games-Howell comparison tests [24], assuming a confidence level of 95% ($p < 0.05$). Statistical analyses were performed with the software R version 3.6.0.

3. Results and discussion

3.1. Intercalation of SDZ in [Mg-Al]-LDH

Initially, the morphology of the commercial [Mg-Al]-LDH was assessed by SEM. The FEG-SEM micrograph of the [Mg-Al]-LDH sample revealed hexagonal-shaped plates, which is a typical morphology of layered double hydroxide particles, as seen in Fig. 1 [25]. The particle diameters ranged from 50 nm to 400 nm, with average value at 150 ± 63 nm.

The structural reconstruction of [Mg-Al]-LDH was evaluated by a series of PXRD measurements (Fig. 2). The PXRD pattern of [Mg-Al]-LDH in Fig. 2-A1 corresponds to hexagonal lattice with rhombohedral 3R symmetry, with basal spacing (d_{003}) of 0.76 nm, which is typical of hydrotalcite [26,27]. After the thermal treatment at 600 °C, the original [Mg-Al]-LDH structure was completely altered, remaining only reflections ascribed to oxides of constituent metals, which indicatives the total collapse of the LDH layered structure (Fig. 2-A2). Once in contact

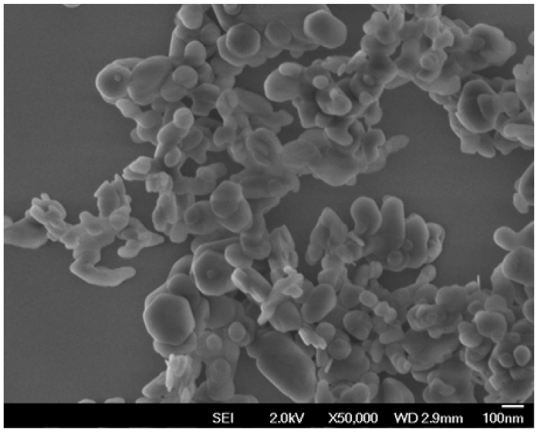

Fig. 1. FEG-SEM image of commercial [Mg-Al]-LDH before thermal treatment.

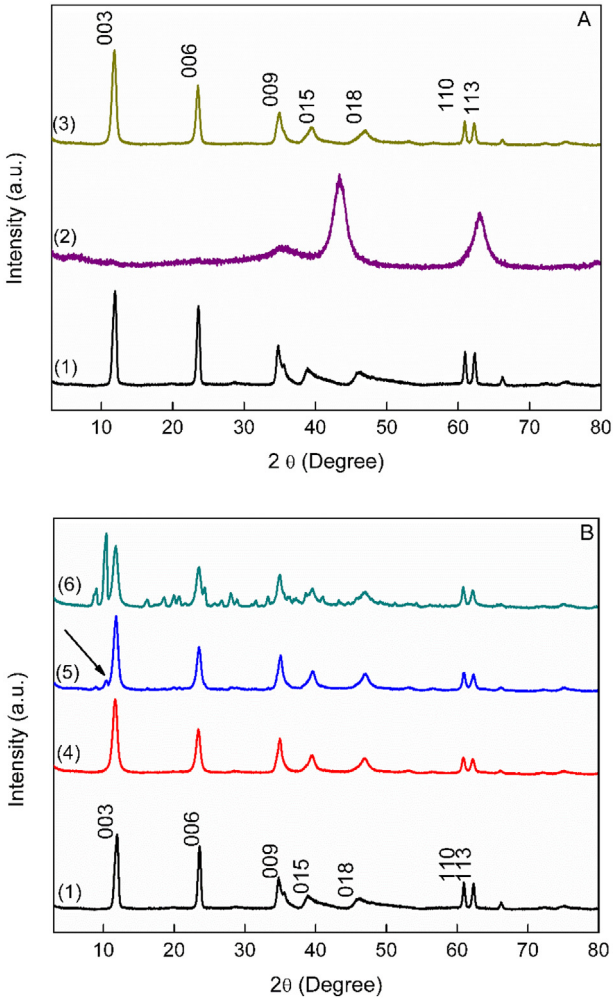

Fig. 2. PXRD patterns of (A) thermal treatment of commercial [Mg-Al]-LDH, (B) SDZ adsorption by [Mg-Al]-LDH at low concentrations, (C) SDZ adsorption by [Mg-Al]-LDH at high concentrations. (1) Commercial [Mg-Al]-LDH, (2) [Mg-Al]-LDH after thermal treatment, (3) [Mg-Al]-LDH after reconstruction in pure water, (4) [Mg-Al]-LDH after reconstruction in 0.008 g L^{-1} SDZ solution, (5) [Mg-Al]-LDH after reconstruction in 0.1 g L^{-1} SDZ solution, (6) [Mg-Al]-LDH after reconstruction in 0.25 g L^{-1} in SDZ solution.

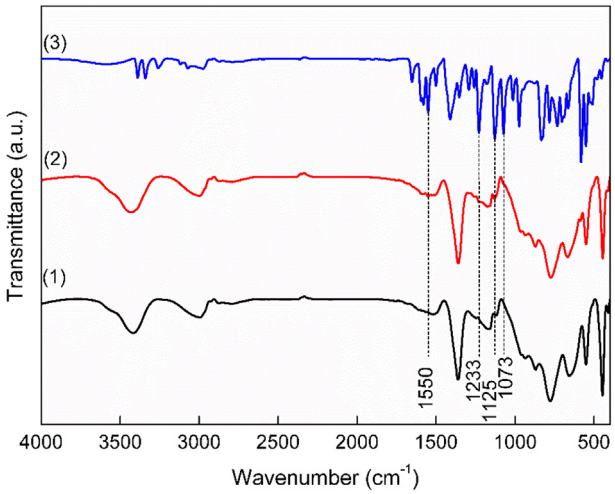

Fig. 3. ATR-FTIR spectra of (1) commercial [Mg-Al]-LDH, (2) [Mg-Al]-LDH after reconstruction in 0.1 g L^{-1} SDZ solution, (3) commercial SDZ.

with pure water, the three-dimensional layered structure was restored, as evidenced in the PXRD pattern in Fig. 2-A3.

Fig. 2-B exhibits the PXRD patterns of the [Mg-Al]-LDH samples after thermal treatment in contact with different SDZ solutions (0.008 g L^{-1}, 0.1 g L^{-1} and 0.25 g L^{-1}). The typical patterns of LDH were well-maintained at low SDZ concentrations, however, from 0.1 g L^{-1}, new reflections at $2\theta = 8.98°$ and $2\theta = 10.19°$ were observed. The reflection at $2\theta = 10.19°$ corresponds to SDZ, which is a crystalline antimicrobial drug, as reported previously [28]. As the initial SDZ concentration increased, the reflection at 10.19° is proportionately intensified, suggesting an excess of SDZ at the external surface of the [Mg-Al]-LDH particles. In contrast, the reflection at $2\theta = 8.98°$ is a new signal, corresponding to a new basal spacing (d_{003}) of 0.99 nm. This indicates that the galleries between the [Mg-Al]-LDH layers expanded to accommodate the SDZ molecules. Therefore, the structural reconstruction was an efficiently route for intercalation of SDZ in [Mg-Al]-LDH.

Overall, the LDH structure was well-maintained and there was minor SDZ excess when the reconstruction process was performed using the 0.1 g L^{-1} SDZ solution. Thus, the sample obtained in this condition was selected for further characterizations by ATR-FTIR, as shown in Fig. 3. Typical vibration bands of [Mg-Al]-LDH can be observed in Fig. 3-1, in particular, an intense band around 3420 cm^{-1}, which is related to O—H stretching vibration of metal hydroxide layer and interlayer water molecules [29]. The presence of CO_2 was evidenced by the band approximately at 1350 cm^{-1}. Bands related with metal oxygen bond stretching were observed at 700 cm^{-1}. SDZ exhibited a peak at around 1550 cm^{-1}, assigned to vibrational stretching of phenyl structures conjugated to NH_2 group and the peak at 1233 cm^{-1} attributed to the S═O asymmetrical stretching. In addition, the bands at 3344 cm^{-1} and 3394 cm^{-1} were assigned to NH_2 stretching [30]. The ATR-FTIR spectrum in Fig. 3-2 represents the interaction of SDZ and [Mg-Al]-LDH, once vibration bands of both materials were identified. However, a decrease in the intensity of the SDZ bands were noticed, especially those assigned to the NH_2 groups, possibly due to the formation of hydrogens bonding with OH groups in the [Mg-Al]-LDH structure [31].

3.2. Antimicrobial properties of [Mg-Al]-LDH/SDZ

Agar diffusion experiments with *E. coli*, *S. enterica* and *S. aureus* sought to give an insight into the antimicrobial activity of [Mg-Al]-LDH/SDZ against Gram-negative (*E. coli* and *S. enterica*) and Gram-positive (*S. aureus*) bacteria. Fig. 4-A shows that the microorganisms were not able to grow due to the presence of the Ag^{+}-containing [Mg-Al]-LDH/SDZ, which has inhibitory action on the bacterial metabolism reactions [32]. Furthermore, the sample powders were deposited at the center of the Petri dishes and inhibition halos were formed for all bacteria most likely due to diffusion of SDZ thought the culture medium. This suggests that SDZ was released from the [Mg-Al]-LDH particles at an amount sufficiently high to inhibit the growth of both Gram-positive and Gram-negative bacteria. In addition, the antimicrobial effect of [Mg-Al]-LDH/SDZ was higher on *S. aureus*, in opposition to the results found by Luan et al. [33] and Thomas et al. [13].

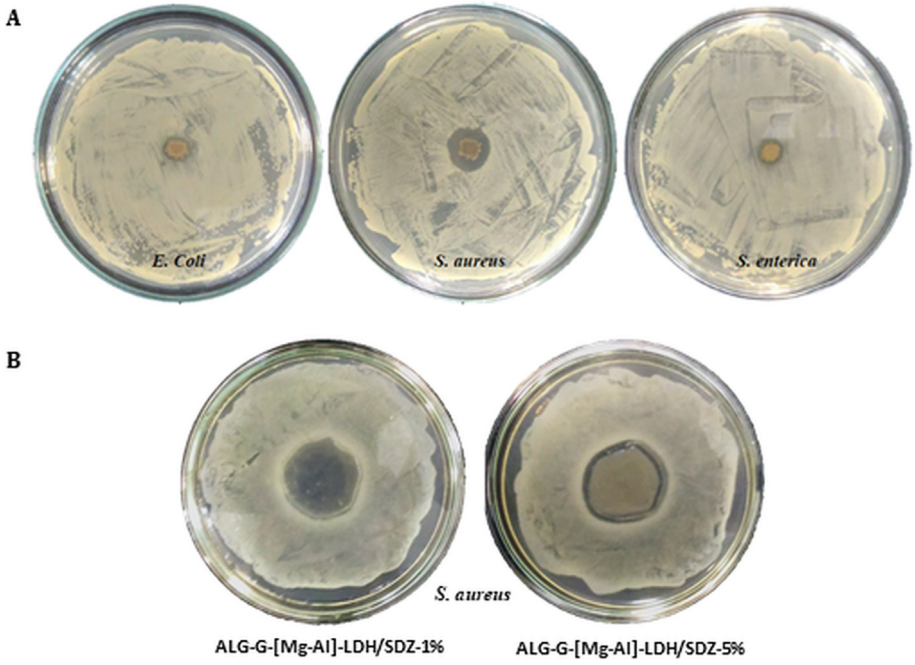

Fig. 4. (A) Bactericidal activity of [Mg-Al]-LDH/SDZ against *Escherichia coli*, *Staphylococcus aureus* and *Salmonella enterica*. (B) Inhibition zones formed by functionalized alginate films against *S. aureus* culture: ALG-G-[Mg-Al]-LDH/SDZ-1% and ALG-G-[Mg-Al]-LDH/SDZ-5%.

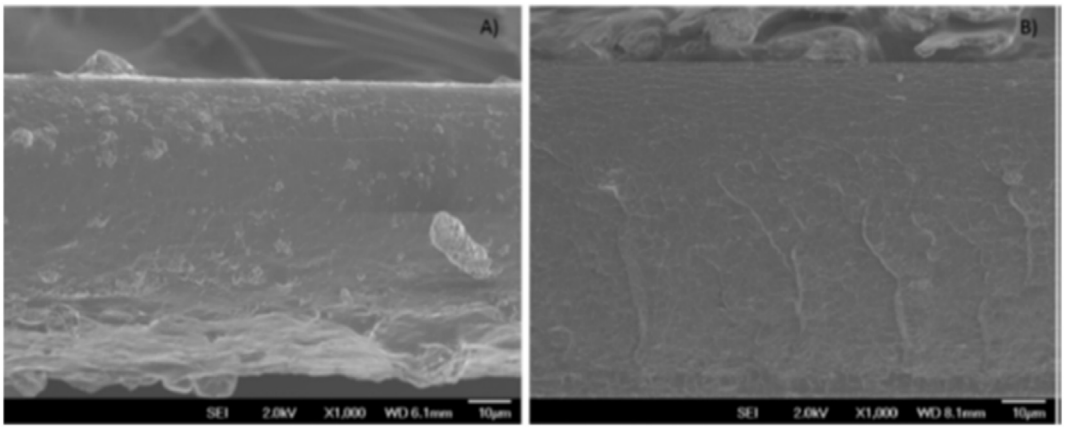

Fig. 5. Cross-sectional FEG-SEM micrographs of (a) ALG-G-[Mg-Al]-LDH/SDZ-1% and (b) ALG-G-[Mg-Al]-LDH/SDZ-5%.

3.3. Antimicrobial activity of alginate films containing [Mg-Al]-LDH/SDZ

The alginate-[Mg-Al]-LDH/SDZ films prepared by continuous casting were first examined in terms of their antimicrobial activity. Inhibition halos were formed when the alginate films containing 1% and 5% [Mg-Al]-LDH/SDZ were placed on the culture medium inoculated with *S. aureus* after 24 h of incubation, as shown in Fig. 4-B. Moreover, the inhibition halo formed by the ALG-G-Mg-Al-LDH/SDZ-5% film was larger than that obtained with the ALG-G-Mg-Al-LDH/SDZ-1% film, which can be explained by the overall larger SDZ content in the former. Similarly, the inhibition halos were also wider when the ALG-G-Mg-Al-LDH/SDZ-5% film was placed on the culture media inoculated with the gram-negative bacteria (Supplementary data- Fig. S1). The ALG-G-Mg-Al-LDH-1% and ALG-G-Mg-Al-LDH-5% films (without SDZ) showed no antimicrobial activity, as expected (results not shown).

Although one of the main differentiations between Gram-positive and -negative bacteria is regarding the presence or absence of an extra, outer cell membrane, this criterion apparently did not play a significant role in the antimicrobial activity of alginate-[Mg-Al]-LDH/SDZ films. According to Jung et al. (2008), the mechanism that drives the antimicrobial action of SDZ is linked to the interaction of the molecule ions to thiol groups in specific cellular enzymes and proteins [34].

It is worldwide known that Ag^+ ions inhibit bacterial growth and are deposited as granules in the vacuoles as well as on the microorganism cell wall. The Ag^+ ion arrange can then damage both cell envelope and bacterial genetic material [35]. Moreover, Ag^+ ions interact with nucleic acids, directly with the DNA bases [36]. Even though application of silver as a biocidal agent has been done since several decades ago, the lethal interaction of SDZ is not well-clarified among the scientific community and certain studies pointed out an negative influence of SDZ in wound healing in rabbits [37].

Recent studies investigated whether silver affected the *quorum sensing* mechanism of bacteria, however, this hypothesis was refused [38]. The authors also pointed out that porins are important in the silver nanoparticle (AgNP) antibacterial mechanism, since Ag^+ ions are smaller than these pores, while AgNP molecules are larger. Thus, the antibacterial activity of AgNP, which present silver ions similarly to SDZ, is resulted from the penetration of silver ions into the cells [35]. Therefore, it is noteworthy that the formation of inhibition zones by the alginate-[Mg-Al]-LDH/SDZ films is probably correlated to the silver ions found in SDZ and the antibacterial activity of these films was positive on the Gram-positive and Gram-negative bacteria, since the Ag^+ ions biocidal action is, apparently, related to mechanisms inside the cells.

3.4. Additional characterizations of the antimicrobial alginate-[Mg-Al]-LDH/SDZ films

The antimicrobial alginate-[Mg-Al]-LDH/SDZ films were further characterized for their morphology, and mechanical and water barrier properties. Fig. 5 shows representative FEG-SEM micrographs of the cross-sectioned surface of the ALG-G-Mg-Al-LDH-5% film. It can be observed that the sample exhibited a compacted and uniform microstructure. Also, there were no areas where the [Mg-Al]-LDH/SDZ particles formed agglomerates. These results suggest that the suitability of the alginate-[Mg-Al]-LDH/SDZ films produced by continuous casting as antimicrobial wound dressing is due to the good dispersion of the [Mg-Al]-LDH/SDZ nanoparticles throughout the alginate matrix. The proper dispersion of the [Mg-Al]-LDH/SDZ in the films could also be related to the proper formation of inhibitory halo in the disc diffusion tests, as observed in Fig. 4-B.

Mechanical properties of alginate-[Mg-Al]-LDH/SDZ films were evaluated by uniaxial tensile tests. True tensile strength (σ_T), true elongation break (ε_B) and Young's modulus (E) are listed in Table 2. Incorporating both [Mg-Al]-LDH and [Mg-Al]-LDH/SDZ into the alginate matrix was not detrimental for the films' tensile properties. In fact, it can be observed that σ_T increased slightly with particle incorporation ($p > 0.05$). A significant reinforcing effect was only observed for the incorporation of [Mg-Al]-LDH/SDZ at 5 wt%, whose σ_T of the corresponding film increased by 60% in relation to the pure alginate film ($p < 0.05$). Similarly, E also increased considerably when [Mg-Al]-LDH/SDZ was added at 5 wt% ($p < 0.05$). On the other hand, ε_B reduced for all samples in

Table 2
Tensile properties (true tensile strength σ_T, true elongation at break ε_B, and Young's modulus E) of alginate-Mg-Al-LDH/SDZ films produced by continuous casting.

Sample	σ_T (MPa)	ε_B (%)	E (MPa)	WVP (g H_2O/m h Pa 10^{-7})
ALG-G (control)	30.6 ± 5.9^a	6 ± 3^a	1857 ± 460^a	2.15 ± 0.78^a
ALG-G-[Mg-Al]-LDH-1%	34.2 ± 4.7^a	$3 \pm 1^{a,b}$	1242 ± 733^a	3.63 ± 0.26^a
ALG-G-[Mg-Al]-LDH-5%	35.9 ± 6.6^a	$3 \pm 1^{a,b}$	1832 ± 540^a	9.69 ± 2.62^b
ALG-G-[Mg-Al]-LDH/SDZ-1%	34.4 ± 8.5^a	2 ± 1^b	2822 ± 398^b	5.29 ± 0.59^b
ALG-G-[Mg-Al]-LDH/SDZ-5%	48.9 ± 6.9^b	$3 \pm 1^{a,b}$	2979 ± 564^b	15.53 ± 1.87^c

ALG = Alginate; G = glycerol 10 wt%; [Mg-Al]-LDH = Hydrotalcite; SDZ = Silver sulfadiazine. Mean values in the same column followed by the same letter are not statistically different at probability level of 5%.

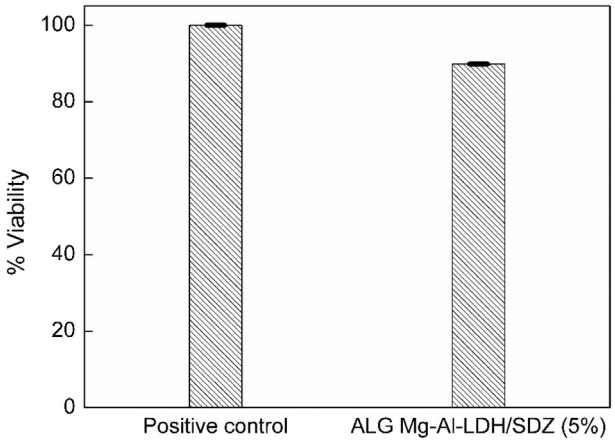

Fig. 6. Indirect cytotoxicity of the ALG-G-[Mg-Al]-LDH/SDZ-5% film on fibroblast cells after 24 h.

comparison to the pure alginate film ($p > 0.05$). These outcomes suggest that a stiffness effect of [Mg-Al]-LDH and [Mg-Al]-LDH/SDZ on the alginate films. The increases in tensile properties provided by [Mg-Al]-LDH/SDZ in relation to [Mg-Al]-LDH may be explained by the fact that the presence of SDZ in the [Mg-Al]-LDH particles improves their interaction with the alginate matrix.

Another fundamental property for an ideal skin scaffold is the water vapor permeability (WVP), since the moisture content is an essential to make available a proper environment for the wound healing process. Large WVP coefficients make possible to create such environment because it prevent the dehydration and accumulation of extra exudates [39]. In this sense, the WVP of the alginate-[Mg-Al]-LDH/SDZ films were also determined and listed in Table 2.

It can be observed that the presence of [Mg-Al]-LDH and [Mg-Al]-LDH/SDZ increased the WVP of the alginate matrix. In particular, the ALG-G-Mg-Al-LDH/SDZ-1% and ALG-G-Mg-Al-LDH/SDZ-5% films showed WVP increased by 246% and 722%, respectively, in relation to the pure alginate film ($p < 0.05$). This may be due to the hydrated structure of [Mg-Al]-LDH, which may have increased the hydrophilicity of the alginate film [40]. Therefore, the ALG-G-Mg-Al-LDH/SDZ-5% film may have adequate properties to keep a balance between preservation and moist evaporation.

3.5. Cell culture and toxicity assay by MTT

The cytotoxicity of the ALG-G-Mg-Al-LDH/SDZ-5% film was examined from the relative cell viability (%) of HDFn fibroblast cells after 24 h incubation (Fig. 6). Silver, either as ions or nanoparticles, may exhibit some cytotoxicity potential [39]. Liu et al. demonstrate that free silver sulfadiazine has a significant reduction effect on the cell viability [41]. It can be seen that the ALG-G-Mg-Al-LDH/SDZ-5% film slightly reduced the relative cell viability by 10% due to the presence of SDZ in its composition. Therefore, the incorporation of [Mg-Al]-LDH/SDZ in alginate films allows, at the same time, proper release of SDZ to provide antimicrobial activity and little significant effect on cell viability. In other words, the alginate-[Mg-Al]-LDH/SDZ films exhibited fine biocompatibility, which is expected to be vital in the fine-tuning of this delivery system for antimicrobial wound dressing applications.

4. Conclusions

Silver sulfadiazine was effectively intercalated in [Mg-Al]-LDH using the structural reconstruction method. Therefore, it can be stated that both materials interacted at the molecular level. Moreover, alginate-based films loaded with properly dispersed [Mg-Al]-LDH/SDZ particles could be produced by continuous casting. Incorporating [Mg-Al]-LDH and [Mg-Al]-LDH/SDZ particles did not alter negatively the mechanical properties of the alginate films but reduced their water barrier properties. Furthermore, the alginate films loaded with 1 wt% or 5 wt% of [Mg-Al]-LDH/SDZ presented inhibitory activity against *E. coli*, *S. aureus* and *S. enterica*, highlighting the antimicrobial potential of the films against gram-positive and gram-negative bacteria. The addition of [Mg-Al]-LDH/SDZ even at the highest concentration (5 wt%) did not afford a very significant cytotoxicity to the alginate-[Mg-Al]-LDH/SDZ films. Therefore, the films developed in this study have promising properties for application as multifunctional wound dressings.

Acknowledgments

The authors are thankful to Embrapa Instrumentation for the laboratorial support, CNPq (grant number 145851/2016-8), FAPESP (grant numbers 2018/07860-90, 2010/11584-5 and 2012/21867-0), Agronano network and SISNANO/MCTI. Also, the authors declare no conflict of interests.

References

[1] A.D. Metcalfe, M.W.J. Ferguson, Tissue engineering of replacement skin: the crossroads of biomaterials, wound healing, embryonic development, stem cells and regeneration, J. R. Soc. Interface (2007) 413–437, https://doi.org/10.1098/rsif.2006.0179.
[2] W. Paul, C.P. Sharma, Chitosan and Alginate Wound Dressings: A Short Review Chitosan and Alginate Wound Dressings: A Short Review, 2015 17–23.
[3] N.J. Percival, Classification of wounds and their management, Surgery (2002) 114–117.
[4] J.S. Boateng, K.H. Matthews, H.N.E. Stevens, G.M. Eccleston, Wound healing dressings and drug delivery systems: a review, J. Pharm. Sci. 97 (2008) 2892–2923, https://doi.org/10.1002/jps.
[5] K. Moore, R. Mccallion, R.J. Searle, M.C. Stacey, G. Harding, Prediction and monitoring the therapeutic response of chronic dermal wounds, Int. Wound J. (2006) 89–96.
[6] M. C, P. M, P. M, E. Krug, A WHO Plan for Burn Prevention and Care, World Health Organization, Geneva, 2008.
[7] M. Tummalapalli, M. Berthet, B. Verrier, B.L. Deopura, M.S. Alam, B. Gupta, Composite wound dressings of pectin and gelatin with aloe vera and curcumin as bioactive agents, Int. J. Biol. Macromol. 82 (2016) 104–113, https://doi.org/10.1016/j.ijbiomac.2015.10.087.
[8] M.D.M. Dantas, D.R.R. Cavalcante, F.E.N. Araújo, S.R. Barretto, G.T.S. Aciole, A.L.B. Pinheiro, M.A.G. Ribeiro, I.B. Lima-verde, C.M. Melo, J.C. Cardoso, R.L.C.A. Júnior, Improvement of dermal burn healing by combining sodium alginate/chitosan-based films and low level laser therapy, J. Photochem. Photobiol. B Biol. 105 (2011) 51–59, https://doi.org/10.1016/j.jphotobiol.2011.06.009.
[9] H. Thu, M.H. Zulfakar, S. Ng, Alginate based bilayer hydrocolloid films as potential slow-release modern wound dressing, Int. J. Pharm. 434 (2012) 375–383, https://doi.org/10.1016/j.ijpharm.2012.05.044.
[10] P. Yadav, H. Yadav, V.G. Shah, G. Shah, G. Dhaka, Biomedical biopolymers, their origin and evolution in biomedical sciences: a systematic review, J. Clin. Diagn. Res. 9 (2015) 21–25, https://doi.org/10.7860/JCDR/2015/13907.6565.
[11] B.A. Aderibigbe, B. Buyana, Alginate in wound dressings, Pharmaceutics 10 (2018) 1–19, https://doi.org/10.3390/pharmaceutics10020042.
[12] N. Agnihotri, V. Gupta, R.M. Joshi, Aerobic bacterial isolates from burn wound infections and their antibiograms — a five-year study, Burns 30 (2004) 241–243, https://doi.org/10.1016/j.burns.2003.11.010.
[13] J.G. Thomas, W. Slone, S. Linton, T. Okel, L. Corum, S.L. Percival, M. Microbiology, In vitro antimicrobial efficacy of a silver alginate dressing on burn wound isolates, J. Wound Care 20 (2005) 124–128.
[14] N. Durán, M. Durán, M.B. de Jesus, A.B. Seabra, W.J. Fávaro, G. Nakazato, Silver nanoparticles: a new view on mechanistic aspects on antimicrobial activity, Nanomedicine Nanotechnology, Biol. Med. 12 (2016) 789–799, https://doi.org/10.1016/j.nano.2015.11.016.
[15] K. Goh, T. Lim, Z. Dong, Application of layered double hydroxides for removal of oxyanions: a review, 42 (2008) 1343–1368, https://doi.org/10.1016/j.watres.2007.10.043.
[16] S.B. Ghorbel, F. Medina, A. Ghorbel, A.M. Segarra, Phosphoric acid intercalated Mg-Al hydrotalcite-like compounds for catalytic carboxylation reaction of methanol in a continuous system, Appl. Catal. A Gen. 493 (2015) 142–148, https://doi.org/10.1016/j.apcata.2015.01.004.
[17] M.P. Bernardo, C. Ribeiro, [Mg-Al]-LDH and [Zn-Al]-LDH as matrices for removal of high loadings of phosphate, Mater. Res. 21 (2018)https://doi.org/10.1590/1980-5373-MR-2017-1001.
[18] S.J. Ryu, H. Jung, J.M. Oh, J.K. Lee, J.H. Choy, Layered double hydroxide as novel antibacterial drug delivery system, J. Phys. Chem. Solids 71 (2010) 685–688, https://doi.org/10.1016/j.jpcs.2009.12.066.
[19] W. Bao, J. Wang, Q. Wang, D.O. Hare, Y. Wan, Layered double hydroxide nanotransporter for molecule delivery to intact plant cells, Sci. Rep. 6 (2016) 1–9, https://doi.org/10.1038/srep26738.

[20] J. Choy, S. Kwak, J. Park, R.V. May, Intercalative nanohybrids of nucleoside monophosphates and DNA in layered metal hydroxide, J. Am. Chem. Soc. 121 (1999) 1399–1400.
[21] M.P. Bernardo, F.K.V. Moreira, L.A. Colnago, C. Ribeiro, Physico-chemical assessment of [Mg-Al-PO_4]-LDHs obtained by structural reconstruction in high concentration of phosphate, Colloids Surfaces A Physicochem. Eng. Asp. 497 (2016) 53–62, https://doi.org/10.1016/j.colsurfa.2016.02.021.
[22] D.R. Munhoz, F.K. Moreira, J.D. Bresolin, M.P. Bernardo, C.P. De Sousa, L.H.C. Mattoso, Sustainable production and in vitro biodegradability of edible films from yellow passion fruit co-products via continuous casting, ACS Sustain. Chem. Eng. 6 (2018) 9883–9892, https://doi.org/10.1021/acssuschemeng.8b01101.
[23] A.W. Bauer, W.M.M. Kirby, J.C. Sherris, M. Turck, Antibiotic susceptibility testing by a standardized single disk method, Am. J. Clin. Pathol. 45 (1966) 493–496.
[24] P.A. Games, J.F. Howell, Pairwise multiple comparison procedures with unequal Nfs and/or variances: a Monte Carlo study, J. Educ. Behav. Stat. (1976)https://doi.org/10.3102/10769986001002113.
[25] C. Puscasu, C. Gherasim, D. Mardare, G. Carja, Study of the textural properties of some layered double hydroxides, ACTA Chem 8 (2013) 1–8, https://doi.org/10.2478/achi-2013-0001.
[26] B. Balcomb, M. Singh, S. Singh, Synthesis and characterization of layered double hydroxides and their potential as nonviral gene delivery vehicles, ChemistryOpen 4 (2015) 137–145, https://doi.org/10.1002/open.201402074.
[27] F. Cavani, F. Trifirò, A. Vaccari, Hydrotalcite-type anionic clays: preparation, properties and applications, Catal. Today 11 (1991) 173–301, https://doi.org/10.1016/0920-5861(91)80068-K.
[28] M. Venkataraman, M. Nagarsenker, Silver sulfadiazine nanosystems for burn therapy, AAPS PharmSciTech 14 (2013) 254–264, https://doi.org/10.1208/s12249-012-9914-0.
[29] F.R. Costa, A. Leuteritz, U. Wagenknecht, D. Jehnichen, L. Häußler, G. Heinrich, Intercalation of Mg – Al layered double hydroxide by anionic surfactants: preparation and characterization, Appl. Clay Sci. 38 (2008) 153–164, https://doi.org/10.1016/j.clay.2007.03.006.
[30] W. Shao, J. Wu, S. Wang, M. Huang, X. Liu, R. Zhang, Construction of silver sulfadiazine loaded chitosan composite sponges as potential wound dressings, Carbohydr. Polym. 157 (2017) 1963–1970, https://doi.org/10.1016/j.carbpol.2016.11.087.
[31] A.R. Fajardo, L.C. Lopes, A.O. Caleare, E.A. Britta, C.V. Nakamura, A.F. Rubira, E.C. Muniz, Silver sulfadiazine loaded chitosan/chondroitin sulfate films for a potential wound dressing application, Mater. Sci. Eng. C. 33 (2013) 588–595, https://doi.org/10.1016/j.msec.2012.09.025.
[32] Y. Zhou, Preparation and antibacterial properties of silver nanowires, Mater. Sci. Forum 944 (2019) 686–691, https://doi.org/10.4028/www.scientific.net/MSF.944.686.
[33] J. Luan, J. Wu, Y. Zheng, W. Song, G. Wang, J. Guo, X. Ding, Impregnation of silver sulfadiazine into bacterial cellulose for antimicrobial and biocompatible wound dressing, Biomed. Mater. 7 (2012)https://doi.org/10.1088/1748-6041/7/6/065006.
[34] W.K. Jung, H.C. Koo, K.W. Kim, S. Shin, S.H. Kim, Y.H. Park, Antibacterial activity and mechanism of action of the silver ion in Staphylococcus aureus and Escherichia coli, Appl. Environ. Microbiol. 74 (2008) 2171–2178, https://doi.org/10.1128/AEM.02001-07.
[35] R. R.M., H.A. Odelola, B. Anderson, Effect of silver on whole cells and spheroplasts of a silver resistant Pseudomonas aeruginosa, Microbios 39 (1984) 157–158.
[36] T.Y. Yoshikuni Yakabe, Takayuki Sano, Ushio Hidrtoshi, Kinetic studies of the interaction between silver ion and deoxyribonucleic acid, Chem. Lett. (1980) 373–376.
[37] L. Qian, A.B. Fourcaudot, K.P. Leung, Silver sulfadiazine retards wound healing and increases hypertrophic scarring in a rabbit ear excisional wound model, J. Burn Care Res. 38 (2017) 418–422, https://doi.org/10.1097/BCR.0000000000000406.
[38] M.A. Radzig, V.A. Nadtochenko, O.A. Koksharova, J. Kiwi, V.A. Lipasova, I.A. Khmel, Antibacterial effects of silver nanoparticles on gram-negative bacteria: influence on the growth and biofilms formation, mechanisms of action, Colloids Surfaces B Biointerfaces 102 (2013) 300–306, https://doi.org/10.1016/j.colsurfb.2012.07.039.
[39] P. Sobhanian, M. Khorram, S. Hashemi, A. Mohammadi, Development of nanofibrous collagen-grafted poly (vinyl alcohol)/gelatin/alginate scaffolds as potential skin substitute, Int. J. Biol. Macromol. (2019)https://doi.org/10.1016/j.ijbiomac.2019.03.045 #pagerange#.
[40] G.I. Olivas, G.V.B.-C. Novas, Alginate – calcium films: water vapor permeability and mechanical properties as affected by plasticizer and relative humidity, LWT - Food Sci. Technol. 41 (2008) 359–366, https://doi.org/10.1016/j.lwt.2007.02.015.
[41] X. Liu, H. Gan, C. Hu, W. Sun, X. Zhu, Z. Meng, R. Gu, Z. Wu, G. Dou, Silver sulfadiazine nanosuspension-loaded thermosensitive hydrogel as a topical antibacterial agent, Int. J. Nanomedicine (2019) 289–300.